EPR Studies in Neutron-Irradiated Silicon: A Negative Charge State of a Nonplanar Five-Vacancy Cluster (V_5^-)†*

Young-Hoon Lee and James W. Corbett
Physics Department, State University of New York at Albany, Albany, New York, 12222
(Received 22 January 1973; revised manuscript received 7 May 1973)

EPR studies are carried out for the float-zone intrinsic silicon irradiated with reactor neutrons up to the total fluence 10^{18} n/cm^2. Details of the Si^{29} hyperfine structure and of the g tensor in the P-1 spectrum are observed with respect to temperature from 77 to 350 °K. The anisotropy of the g tensor and its continuous variation with temperatures are also discussed in terms of simple linear-combination-of-atomic-orbitals molecular orbitals and of the experimental results on the resonant wave function. In particular, the motional effect due to the electron-hopping between equivalent defect sites proposed by Nisenoff and Fan is not supported by these experiments, but an unusual thermal effect is observed in which the resonant-electron wave function is an average of both a ground and excited states, with the relative populations being proportional to the Boltzmann factor. The resonance properties of the pure ground state and pure excited state differ, which causes the g and A tensors to continuously vary with temperature and brings about a line broadening and narrowing in the hyperfine satellites as well as in the central lines. The line width broadening of the hyperfine lines is discussed on the basis that it is mainly due to transitions between the ground and excited electronic states. Based on the present results, a defect model for this center is established: a negative charge state of a nonplanar five-vacancy cluster.

I. INTRODUCTION

A number of paramagnetic resonance studies have been undertaken on paramagnetic defect centers in neutron-irradiated silicon. Although a variety of simple defect centers have been observed and unambiguously identified in electron-irradiated silicon,[1,2] few of the known spectra which are almost solely produced by neutron bombardment have been understood sufficiently enough to establish a microscopic model.

The present study extends the previous EPR work[3,4] on the previously identified spectrum, Si-P-1 [or Si-N center in Ref. (3)], particular emphasis being on the temperature dependence of its EPR parameters, both g and A tensors. (Since all of the spectra treated in this paper are in silicon we will hereafter omit the Si prefixes.)

Three distinct Si^{29} hyperfine systems are unraveled at high temperature, in addition to the one observed by Nisenoff and Fan[3] at low temperature near 77 °K. Details of the Si^{29} hyperfine structure lead us to construct a physical model of the P-1 center, which, in turn, provides a satisfactory explanation for the temperature dependence of g tensor.

We briefly describe the procedures of our experiment in Sec. II, and then present the new EPR data associated with the P-1 spectrum in Sec III. In Sec. IV, the microscopic model of the P-1 center as a nonplanar five-vacancy cluster is discussed, including a comparison to the g values of previously identified centers which comparison argues that the resonance is observed in the negative charge state. It is argued that the unusual, marked temperature variation in the hyperfine and g-tensor parameters arises from transitions between the ground state and first excited state. It is shown that in addition to these features the response of the spectra to an external ⟨110⟩ compressional stress is also consistent with the model. Section V is a summary.

II. EXPERIMENTAL PROCEDURE

The samples studied in this experiment are from three boules of float-zone silicon (intrinsic, P doped and B doped). The intrinsic sample whose impurity concentration is less than 10^{12} atom/cm^3 is primarily used to study the P-1 spectrum, but the other two provide the same spectra over the entire temperature range we have studied. Each crystal was oriented by x-ray diffraction and cut to the size cross section 0.1×0.1 in. with length 1.0 in. along the ⟨110⟩ crystal axis.

The irradiation was performed at room temperature using the reactor at Oak Ridge National Laboratory with a total fluence of 10^{18} n/cm^2. After irradiation, the sample was etched in a chemical solution (HNO_3 60%, HF 40%) until the broad EPR absorption line arising from surface damage completely disappeared.

EPR measurements were made with Varian spectrometers at X band (9.5 GHz) and at Q band (35.0 GHz). Temperature variation between 77 and 350 °K was made by utilizing the Varian temperature controller and was monitored with a copper-constantan thermocouple on the cavity.

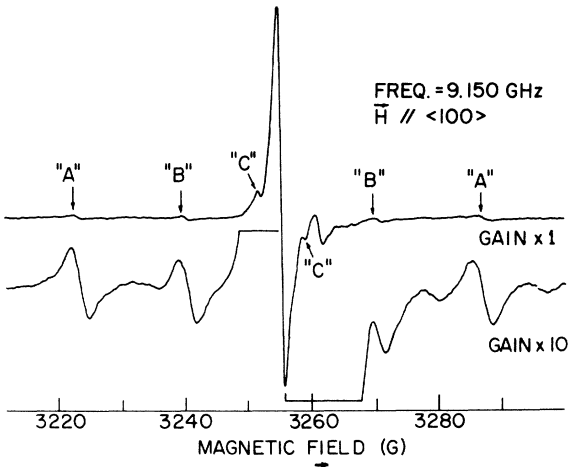

FIG. 1. P-1 spectrum with $\vec{H} \| <100>$; the measurement was made at 300 °K with the sample annealed at 270 °C for 30 min where the resonance signal reaches its maximum. Three weak lines A, B, and C are the hfs satellites associated with the Si^{29} isotope.

III. EXPERIMENTAL RESULTS

A. Previous Work on the P-1 Spectrum

The P-1 spectrum is known to be one of the dominant paramagnetic centers in either neutron or ion bombarded silicon. Although a great deal of effort has been devoted to understanding this center, the previous results[3] were not sufficient to construct a physical model of the defect. We briefly summarize the previous results.

(i) P-1 was first observed in neutron-irradiated silicon with high fluence > 10^{17} n/cm^2. It does not appear in the initial state of irradiation. It is observed only after annealing at 170 °C, and is independent of doping impurity. It disappears upon annealing at ~450 °C.

(ii) The magnitude, as well as the orientation, of the principal g values vary continuously with temperature between 104 and 350 °K, but no temperature dependence was observed between 4.2 and 104 °K. Near 104 °K, it was thought (but see below) that some of the central lines vanish and corresponding new lines emerge without changing the symmetry of g tensor. This was interpreted in terms of "electron hopping" between two particular defect sites whose g_2 axes are aligned in the same ⟨110⟩ direction and g_1 axes are shifted by $\pm\theta°$, respectively, from another ⟨110⟩ crystal axis. It was also suggested that, at $T \simeq 160$ °K, the thermal average of lattice distortions in the vicinity of the defect results in a continuous variation of the g tensor with temperature.

(iii) At both 77 and 4.2 °K, one set of hyperfine structure associated with the Si^{29} isotope was resolved, but not at any other temperature. Analysis indicated that 63% of total wave function is localized in a dangling bond, giving rise to a resonance whose g and A tensors are nearly axial symmetry along the ⟨111⟩ axis.

B. EPR Spectrum

Figure 1 shows the P-1 spectrum for the external magnetic field $\vec{H}$ parallel to the ⟨110⟩ crystal axis, showing the strong central line and the newly observed sets of hyperfine satellites labeled as A, B, and C, due to the isotope Si^{29} (natural abundance 4.7%, nuclear spin $\frac{1}{2}$) in the vicinity of defects. The P-1 spectrum requires the spin Hamiltonian

$$\mathcal{H} = \mu_B \vec{H} \cdot \overleftrightarrow{g} \cdot \vec{S} + \sum_j \vec{I}_j \cdot \overleftrightarrow{A}_j \cdot \vec{S} \qquad (1)$$

with $S = \frac{1}{2}$, in order to describe the angular variation of the spectrum. The first term represents the electronic Zeeman interaction and the second term, the magnetic hyperfine interaction with nuclei at jth site, with the summation over all possible nonequivalent positions.

In Fig. 2, we show the angular variation of the P-1 spectrum at 320 °K, except for the C hfs satellite. The solid lines represent the central lines, and the set of dotted lines and the set of dashed

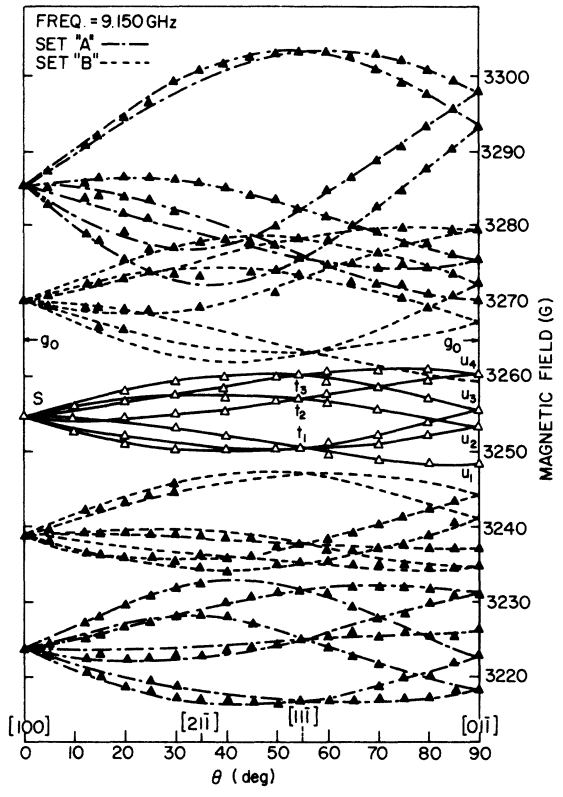

FIG. 2. Angular dependence of the P-1 spectrum in the {110} plane (T = 320 °K); the lines are from theoretical calculation and the experimental points were taken at X band. Two sets of the Si^{29} hyperfine structure are also given.

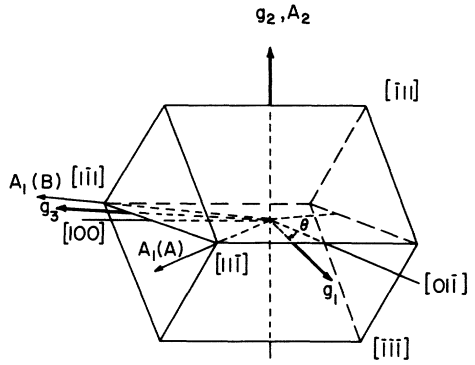

$g_1 = 2.0050 \pm 0.0003$
$g_2 = 2.0127 \pm 0.0003$
$g_3 = 2.0091 \pm 0.0003$
$\theta = 15°$

hfs "A"
$A_1 = 80.9 \times 10^{-4}$ cm^{-1}
$A_2 = 41.7 \times 10^{-4}$ cm^{-1}
$A_3 = 41.7 \times 10^{-4}$ cm^{-1}
$\theta_A = 35.5°$

hfs "B"
$A_1 = 40.7 \times 10^{-4}$ cm^{-1}
$A_2 = 21.0 \times 10^{-4}$ cm^{-1}
$A_3 = 21.4 \times 10^{-4}$ cm^{-1}
$\theta_B = -34°$

FIG. 3. Geometry and axes of the principal coordinates and the EPR parameters at 320 °K.

lines, symmetrically located around the central lines, describe the angular variation of hyperfine structure. The data points fit very well the theoretical predictions made with Eq. (1), the EPR parameters and the axes given in Fig. 3. For later discussion, we have labeled central lines in the three crystal axes as s at ⟨100⟩, t_1, t_2, t_3 at ⟨111⟩, and u_1, u_2, u_3, u_4 at ⟨110⟩, respectively. We do not present the 77 °K results, since they are identical to those given by Nisenoff and Fan.[3]

Only the A and B hyperfine lines could be followed from the ⟨100⟩ to the ⟨110⟩. The C hyperfine structure was clearly observed in many orientations, but it has not been possible to unravel its anisotropy. The intensity ratio of the hyperfine satellites to the corresponding central lines was measured at those orientations where the lines are well isolated. Both A and B satellites have the relative intensity 2.4%, as expected if only one nucleus is involved in the interaction, while the ratio for the set C ranges from 15 to 18%, consistent with the assignment of six or seven equivalent nuclear sites.

We have studied the temperature dependence of both g and A tensors in the temperature range between 77 and 350 °K. Figure 4 shows the variation of the principal g values and of the distortion angle (θ) with temperature from 77 to 350 °K. Measure-

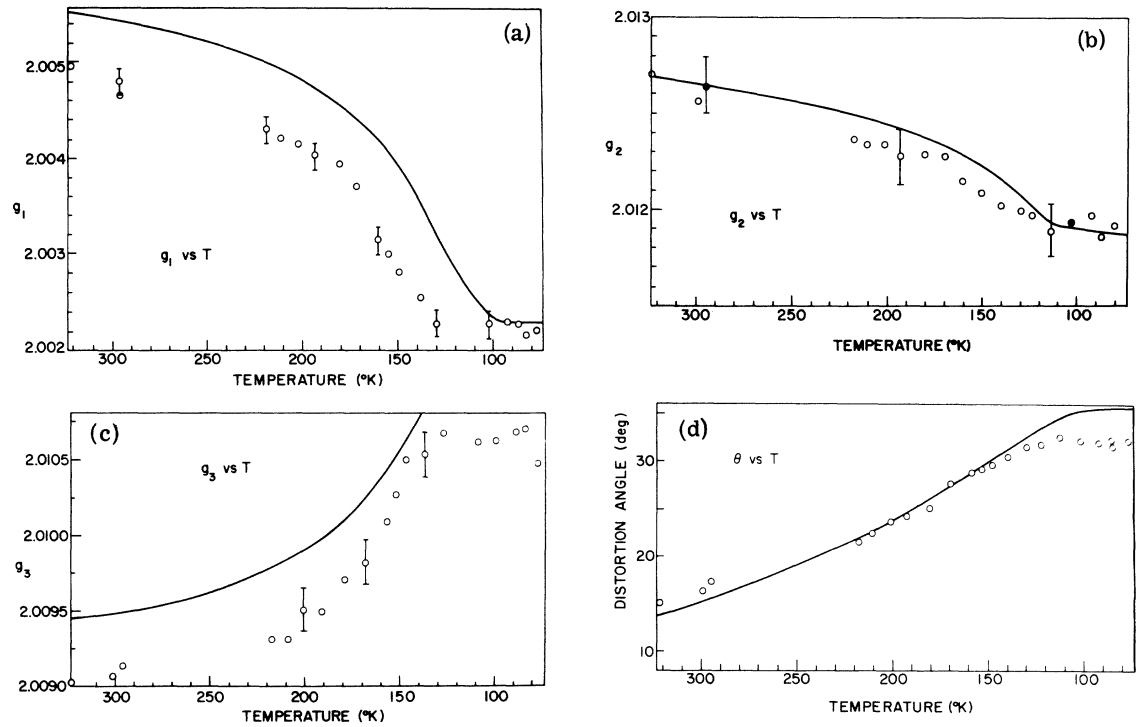

FIG. 4. Temperature dependence of the g tensor; (a) g_1 vs T, (b) g_2 vs T, (c) g_3 vs T, and (d) θ vs T. Solid line is a theoretical prediction, in which the parameters (K and K') are determined from the g_2 values (filled circles) at 100 and 300 °K (see Sec. IV D 2).

ments were made at X band and at Q band. The least-squares method, primarily developed by Jung, [5] was applied to calculate the principal values and angle. The present measurement shows that the g values vary continuously with temperature down to ~100 °K and then reach a plateau where the g values are independent of temperature, in disagreement with the previous results which argued that the g tensor undergoes a discontinuous change near 104 °K. We will fully discuss this point in Sec. IV B.

As shown in Fig. 5, we have also observed three sets of the Si^{29} hyperfine structure that vary with temperature in the same temperature interval of 100–370 °K. The character of temperature dependence can be divided into three regions in terms of temperature: (a) region I (200–370 °K), where the hyperfine separation of the satellite A from the corresponding central line increases linearly from 30 G at 370 °K to 35 G at 200 °K, while that of the satellite B decreases from 17 G at 370 °K to 11 G at 200 °K in the same fashion; (b) region II (100–200 °K) where both satellites A and B undergo a rapid change in the hfs separations as well as the linewidth; and (c) region III (4.2–100 °K) where no further change occurs. For the satellite C, the change in $A(100)$ with temperature is small, but we could clearly see the increase in $A(100)$ from 3 G at 320 °K to 5 G at 77 °K, with the estimated error range (±0.5 G). Satellite B could not be traced below 170 °K, because (i) it is obscured by the strong C line, and (ii) a severe line broadening takes place in the B line. The hfs line B seems to gradually approach the corresponding central line and to combine with it near 110 °K. The satellite A could be traced down to 77 °K, though it also undergoes a line broadening and narrowing in the region II. Further details on the linewidth of the satellite A will be described in Sec. IV C.

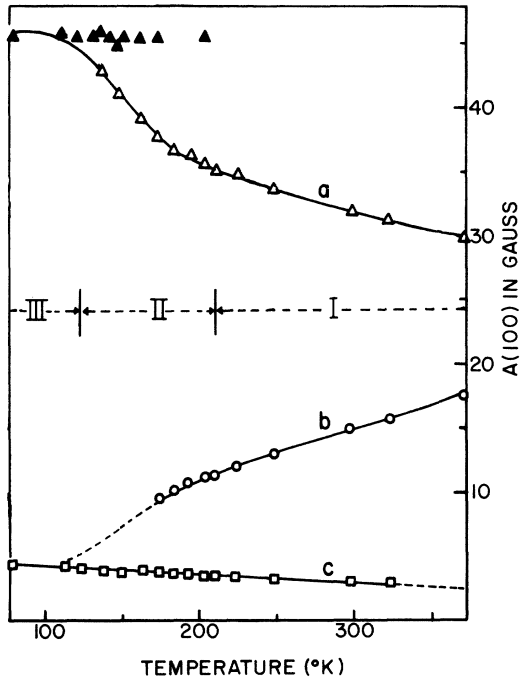

FIG. 5. Hyperfine splittings [$A(100)$] versus temperature ($\vec{H} \| < 100 >$); the line a (open triangles) refers to the variation of the hfs satellite A in Fig. 1, the line b (circles) is for the satellite B, and the line c (squares) for the satellite C. Filled triangles near the line a represent the hfs line corresponding to the one at 77 °K which appears simultaneously with the satellite A (open triangles) at that temperature.

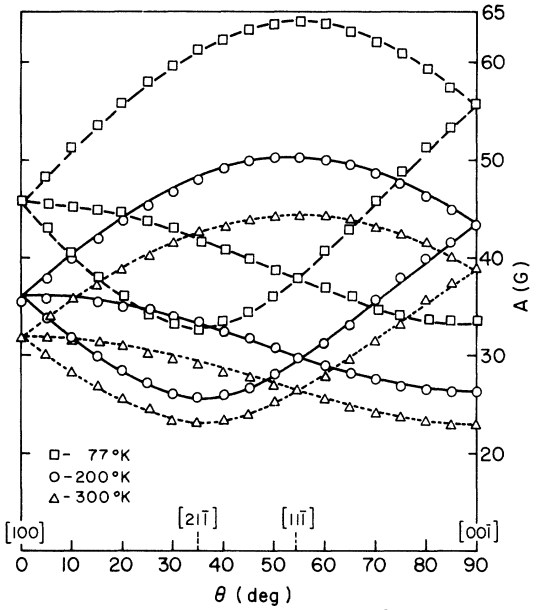

FIG. 6. Angular dependence of the Si^{29} hyperfine structure (set A); (a) the dotted lines (triangles) are at 300 °K (b) the solid lines (circles) at 200 °K, and (c) the dashed lines (squares) at 77 °K. The anisotropy of the A tensor shows ⟨111⟩ axial symmetry, regardless of temperature.

We present in Fig. 6 the angular variation of the hyperfine structure of the set A at various temperatures. Here we superimpose the rotation patterns at three different temperatures, in order to show the temperature dependence of the A anisotropy. The A tensor always has ⟨111⟩ axial symmetry, with $A_{\|}$ directing to [11$\bar{1}$] axis for the particular defect in Fig. 3, regardless of temperature, only its magnitude varying with temperature. The hyperfine structure of the set B, closer to the central lines, could not be resolved completely at every orientation, but a partial resolution at three crystallographic axes (the hfs splitting of the central line s at ⟨100⟩, those of the lines t_1, t_2, and t_3 at ⟨111⟩ and those of u_1 and u_2 at ⟨110⟩) enables us to calculate the principal values and their direc-

TABLE I. Hyperfine structure of the P-1 spectrum (the unit is in 10^{-4} cm^{-1}).

Temp. (°K)	$A_1(A)$	$A_2(A)$	$A_3(A)$	θ_A°	$A_1(B)$	$A_2(B)$	$A_3(B)$	θ_B°
320	81.1	42.6	43.0	35.1	41.5	22.8	21.3	−34.1
300	83.0	43.5	43.5	35.2	38.8	21.5	21.3	−35.0
273	85.5	44.8	44.5	35.0	36.5	19.9	19.4	−36.4
250	87.4	45.8	45.3	35.5	34.6	19.5	18.5	−36.0
230	90.4	47.7	46.7	35.2	30.3	18.5	19.3	−34.0
210	91.8	48.9	47.3	35.9	29.3	17.4	18.2	−34.0
200	94.1	49.2	47.9	35.6	27.9	16.1	16.8	−36.0
180	95.7	51.3	49.8	35.8	26.4	15.2	11.2[a]	−38.9[a]
160	102.2	57.7	54.1	35.4	• • •	• • •	• • •	• • •
120	118.4	63.1	62.9	35.1	• • •	• • •	• • •	• • •
110	119.7	62.6	62.5	35.0	• • •	• • •	• • •	• • •
77	119.4	62.5	62.2	35.1	• • •	• • •	• • •	• • •

[a]The considerable error was expected, since the satellites approach to the corresponding central lines.

tions by utilizing the "least-squares method."[5] The hyperfine tensor of B is directed roughly 109° from $A_{\parallel}$ of the set A in the same {110} plane; i.e., $A_{\parallel}$ of B lies along the $[1\bar{1}1]$ axis in Fig. 3. The results for both set A and B are listed in Table I. We note here that the angles, θ_A and θ_B, are independent of temperature.

IV. DISCUSSION

A. Model

In Fig. 7 we present a model of the defect giving rise to the P-1 spectrum. It is a five-vacancy cluster, an impurity-independent defect having C_{1h} ($=C_s$) symmetry. A string of three adjacent vacancies V_1, V_2, and V_3 is aligned in the $[01\bar{1}]$ axis, with two more vacancies V_4 and V_5 sitting at both sides of the end vacancy (V_3) along the [011] axis, i.e., perpendicular to the string of vacancies ($[01\bar{1}]$ axis). The electronic structure of this defect derived from a simple linear-combinations-of-atomic-orbitals (LCAO) molecular orbital treatment is illustrated in Fig. 8 assuming that the energy separation between the bonding and antibonding orbitals varies roughly inversely with the distance between two interacting orbitals. The orbitals due to atoms A and B are not equivalent and the energy of that for B is assumed to be lower.

We argue that the P-1 center is due to a negative charge state by comparing it to centers in which the responsible defect has been identified. In Fig. 9, we plot all the known silicon radiation-defect paramagnetic centers in terms of their g shifts $\Delta g_{\parallel}$ and $\Delta g_{\perp}$. (If the g tensor was not axially symmetric, we either averaged two approximately equal values to get $g_{\perp}$, naming the other component as $g_{\parallel}$, or if the differences in magnitude among three principal g values were comparable, we chose the largest

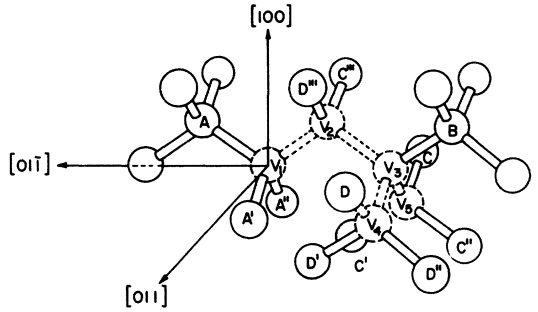

FIG. 7. Physical model of five-vacancy cluster; V_1, V_2, V_3, V_4, and V_5 refer to the five vacancies involved and A, A', B, D, etc., are silicon atoms adjacent to the vacancies. There is only one reflection plane, the (011) plane.

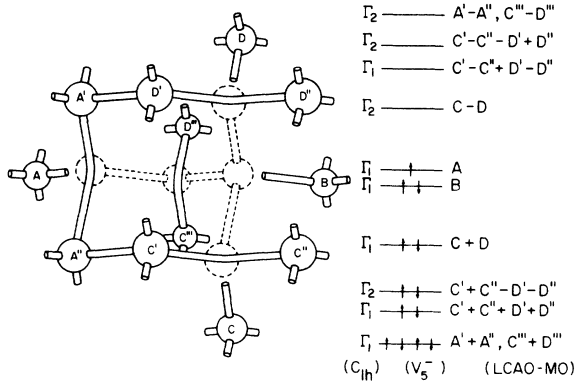

FIG. 8. Electronic structure of the five-vacancy cluster; the "extended pair bond" is assumed to form between two close-by broken bonds such as $A'+A''$ and $D'+D''$. A, B, C, etc., represent simply LCAO-MO orbitals corresponding to the broken bonds of the atoms A, B, C, etc., and group-theoretical arguments were used to predict the energy levels.

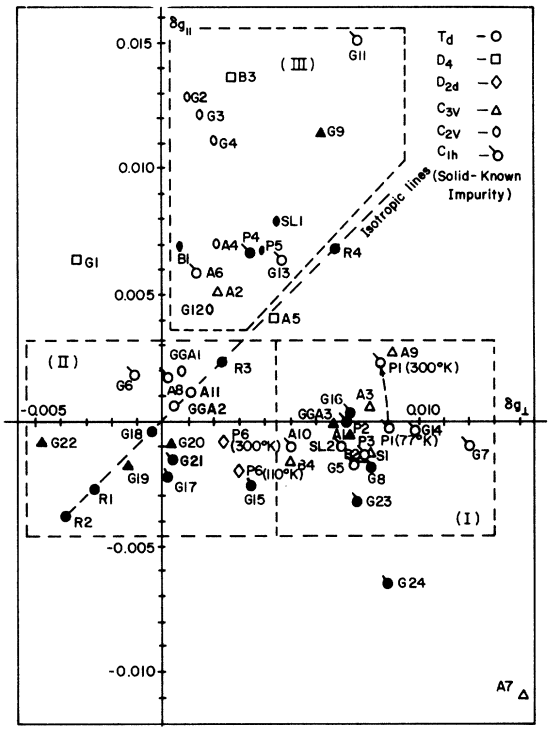

FIG. 9. EPR spectra in irradiated silicon; the spectra are classified in terms of their g shift and symmetry (see text). The impurity-associated spectra are presented with solid marks. We follow the nomenclature suggested by Watkins (Ref. 1) to designate the EPR spectra: *A* spectra (Refs. 6 and 7), *B* spectra (Refs. 1, 8, 9, and 10), *G* spectra (Refs. 1 and 11), *GGA* (Ref. 12), *P* (Refs. 3 and 4), *R* (Refs. 13 and 14), *S* (Ref. 15), and *SL* (Refs. 16 and 17).

one as $g_{\parallel}$ and averaged the other two to get $g_{\perp}$.) By examining the position of the established centers we notice that the EPR spectra are grouped by the symmetry of the g tensors and their charge states. First, the centers with the resonant electron primarily in one ⟨111⟩ dangling bond [vacancy +phosphorus (*G*-8), +arsenic (*G*-23), and +antimony (*G*-24)] and those with two parallel ⟨111⟩ bonds [divacancy (*G*-6 and *G*-7) and four-vacancy (*P*-3 and *SL*-2)] cluster together, while the centers with the "bent-pair" bonds, i.e., the electron primarily in ⟨111⟩ bonds 109° from each other, form another group [vacancy (*G*-1 and *G*-2), vacancy+oxygen (*B*-1 and *SL*-1), and vacancy+aluminum (*G*-9)]. Second, a negative charge state has a large positive g shift in the $g_{\perp}$ component, while a positive state contributes less to the g shift so that $\Delta g_{\perp}$ becomes either negative or nearly zero. For example, the divacancy center[18] is known to produce the two distinct spectra of different charge states; the *G*-7 spectrum, a negative charge state, has a large positive $\Delta g_{\perp}$, whereas the *G*-6, a positive charge state, has a negative shift in $\Delta g_{\perp}$. This can be also seen from the two charge states (*G*-1 and *G*-2) of a single vacancy center. Therefore, we see that all the EPR spectra in irradiated silicon in Fig. 9 tend to divide into three distinct groups: (a) group I, a negative charge state of a broken bond and of parallel pair bonds ($\Delta g_{\parallel} \simeq 0$ and $\Delta g_{\perp} > 0$); (b) group II, a positive charge state of a broken bond and of parallel pair bonds ($\Delta g_{\parallel} \simeq 0$ and $\Delta g_{\perp} \lesssim 0$); and (c) group III, a bent-pair bond ($\Delta g_{\parallel} > 0$ and $\Delta g_{\perp} > 0$).

It is clear therefore, that *P*-1 is more likely to be negative charge state than a positive state. As indicated in Fig. 9, *P*-1 moves with temperature from the region where the negatively charged dangling bond centers are mostly concentrated toward the region where the bent-pair bonding centers are. This is consistent with the model. We will also argue (Sec. IV D) that the temperature dependence of the g tensor indicates a negative charge state.

This model satisfies many of the essential features deduced from the EPR spectrum: (i) At low temperatures near 77 °K, the unpaired electron is mostly localized in a dangling bond (the orbital A) associated with the single atom A, so that the g tensor becomes nearly axially symmetric and the $g_{\parallel}$ axis is parallel to the $A_{\parallel}$ axis along the same ⟨111⟩ direction. (ii) As temperature increases to ~300 °K, the resonant electron is no longer localized in a single atom, but rather is shared by the two atoms A and B through thermal excitation; thus, the resonant wave function is asymmetrically distributed between these two bonding orbitals A and B, giving rise to two unequal sets of the Si^{29} hyperfine structure. (iii) The hyperfine axes reflecting the ⟨111⟩ axis of the broken bonds at each site make the angle close to 109° at a high temperature near 300 °K, because three vacancies along the ⟨110⟩ axis are involved. (iv) Since the defect is formed by a five-vacancy cluster, we argue it can be stable even after the loss of the divacancy at 350 °C. (v) The {110} symmetry of the defect is consistent with the symmetry of the g tensor. In fact, this model can explain all the characteristics of the *P*-1 spectrum we have found in our experiments. In Sec. IV B we will compare our results to those of Nisenoff and Fan. In subsequent sections we analyze the EPR parameters in more detail.

B. Temperature Dependence

In this section we discuss our observations of the temperature dependence of the *P*-1 spectrum including the hyperfine spectrum which prove incisive in sorting out the discrepancies between our results and those indicated by Nisenoff and Fan.[3] They reported that, near 104 °K, certain central lines (the lines t_2, t_3 at ⟨111⟩ and u_2, u_3 at ⟨110⟩ in

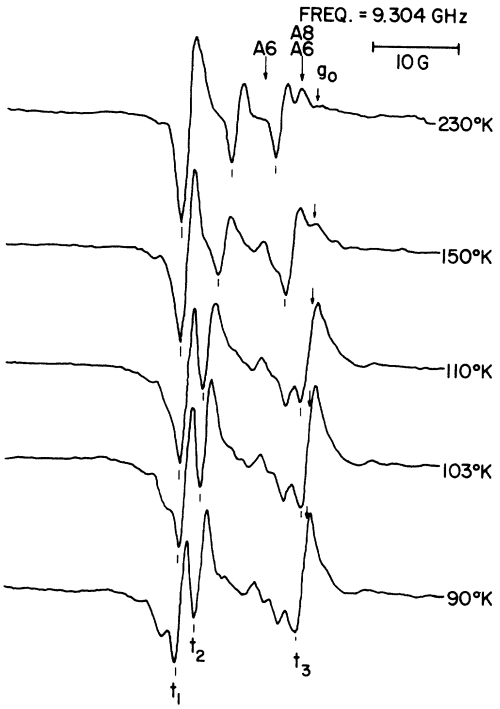

FIG. 10. Temperature dependence of the central lines at $\vec{H} \| <111>$; three lines, labeled as t_1, t_2, and t_3 (cf. Fig. 2), can be followed from 77 to 350 °K. We note that, at $T = 103$ °K, the t_2 and t_3 lines do not vanish, contrary to the previous result by Nisenoff and Fan. Other weak absorption lines belong to either A-6 or A-8.

Fig. 2) vanish and new lines appeared above that temperature, owing to "electron hopping"—electronic motion between equivalent defect sites. Contrary to their report, we have not seen any indication of central lines *vanishing* at all. Figure 10 shows a variation of the P-1 spectrum with temperature, when the magnetic field is parallel to the ⟨111⟩ axis. The spectra were taken at X band (9.5 GHz), with particular attention to temperatures near 104 °K. We chose a sample which had been annealed at 400 °C, in order to avoid the presence of other strong spectra[6] like A-2 and A-3, etc. Both A-6 and A-8 still appear in the range near $g = 2.0$. As shown in Fig. 10, movement of the lines t_2 and t_3 with temperature can be clearly observed, evan at 104 °K. Measurements were also made at other orientations, ⟨211⟩ and ⟨110⟩, in which no sign of disappearance of lines were observed. If the disappearance of central lines that Nisenoff and Fan say they observed were truly caused by electron jumping only between two particular equivalent defects which have common g_2 axis along the same ⟨110⟩ axis, as they claimed, it should give rise to a motionally averaged state as well as motional broadening effect in a higher temperature. Watkins and Corbett[18,19] have observed many instances of centers in electron-irradiated silicon with motional effects arising from electrons hopping between equivalent sites. If this were the case for P-1, the motional average of the t_2 and t_3 lines at $\vec{H} \| \langle 111 \rangle$ would give rise to one line at a middle of the two and the intensity of a new line should be comparable to that of t_1. With $\vec{H} \| \langle 110 \rangle$, likewise, the u_2 and u_3 lines would average out to bring about one new line at a center between u_2 and u_3. We would therefore end up with such configuration of principal g axes that g_1 and g_3 are aligned in the ⟨110⟩ and ⟨100⟩, respectively; i.e., the g tensor in motional average state should have a C_{2v} symmetry. Contrary to this prediction of motional effect, they observed, as do we, a change in g tensor with temperature, keeping the same symmetry C_{1h}.

In order to interpret the previous measurement by Nisenoff and Fan, we need first to describe in detail what we have seen in the hyperfine structure. In Fig. 11 we show a sequence of actual EPR

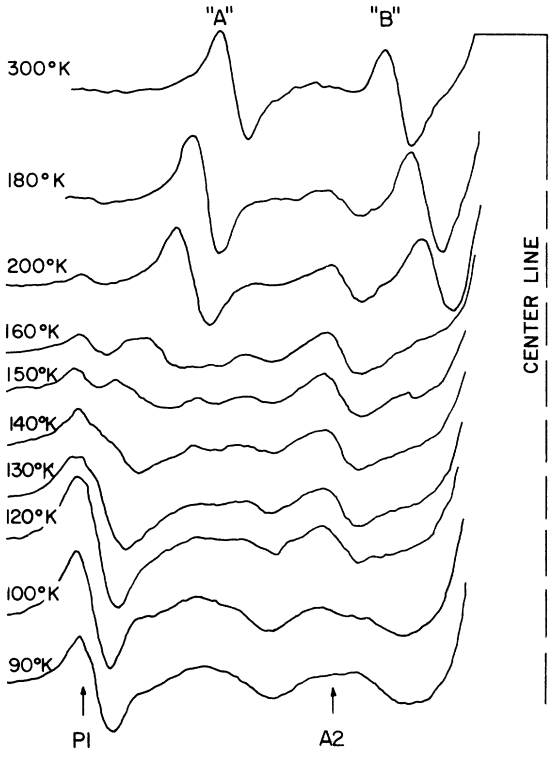

FIG. 11. Temperature dependence of the hyperfine satellites as $\vec{H} \| <100>$; at 90 °K, the set B is no longer observed and the set A, denoted as P-1 with arrow, can be only observed. $A2$ indicates the hfs line associated with the A-2. In the temperature interval of 100—200 °K, the set A splits into two lines, one being associated with the lower temperature line ($P1$) and the other corresponding to the hfs line at the higher temperature. Both intensity and linewidth is also changing with temperature in the same range.

spectra of the hyperfine satellites A and B at various temperatures with $\vec{H} \parallel \langle 100 \rangle$. (Since a hyperfine line reflects the wave function at a specific-type atom we will use A and B to label both lines and atoms.) The separation of these hfs lines from the central line were given in Fig. 5, where the temperature interval is divided into three regions, I, II, and III. The general trend has the electron solely on the A atom at 77 °K (i.e., maximum splitting in the A atom hyperfine) with a uniform transfer with increasing temperature to atom B (i.e., a decrease in the A hyperfine splitting and the appearance of B and increase in B splitting). In addition the hyperfine spectra clearly exhibit line broadening (see Sec. IV C); at 77 °K, the A line is sharp; as the temperature increases the A line broadens, the A-like motionally averaged line appears and then narrows. We will consider the temperature dependence of the hyperfine parameters in Sec. IV C.

Equivalent effects are seen in the central lines. As the temperature increases, the central lines t_2, t_3 at the $\langle 111 \rangle$ direction and u_2, u_3 at the $\langle 110 \rangle$ show line broadening, considerably reducing their intensity, and split into two lines which correspond to the ground state and the averaged state, respectively. The clear resolution of both lines, the ground state and averaged lines, can be achieved in the Q-band (35-GHz) measurements. The rest of the lines, t_1, u_1, and u_4, stay sharp regardless of temperature. At X band the separation between lines is too small to observe the two lines, but rather they are superimposed on each other, behaving like one broadened line as shown in Fig. 10. This is presumably what led Nisenoff and Fan, who measured at K band (24 GHz), into arguing that four lines (t_2, t_3, u_2, and u_3) disappeared.

In summary then our model of the temperature dependence is that it is due to transitions between the ground state and first excited state of the defect. The resonant properties of the two states differ. At low temperatures the resonant electron is in the ground state and the corresponding spectrum ensues. Upon increasing the temperature, transitions between the ground and excited states occur, causing a lifetime broadening on the ground-state spectrum. When the transition rate is fast enough the spectrum reflects a resonant wave function which is an average of the ground- and excited-state wave functions, the relative proportions given by the Boltzmann factor. Consequently, with increasing temperature one passes from the regime with a broadening and diminution of the ground-state spectrum to a regime where the average spectrum appears and narrows. The one discrepancy with the model is that we observe a regime in which *both* the broadening ground-state line and the narrowing averaging line are observed. It is not clear whether the simultaneous observation of both the ground and averaged states is a natural consequence of a motional effect or due to internal strains in the lattice causing the $E_A - E_B$ energy difference to vary slightly. It requires further studies to unravel.

C. Hyperfine Interactions

Watkins and Corbett[19] have analyzed the hyperfine interactions in terms of the Fermi contact term (a_j) and the magnetic dipole-dipole term (b_j) by constructing ($3s$, $3p$)-hybrid orbitals given by

$$\Psi = \sum_j \eta_j (\alpha_j \phi^j_{3s} + \beta_j \phi^j_{3p}) . \tag{2}$$

Here, η_j^2 represents a fractional contribution to the interaction by jth site and the atomic orbital at each nuclear site j is normalized as $\alpha_j^2 + \beta_j^2 = 1$. With these bases, the principal values of an axially symmetric A tensor are given by

$$A_{\parallel}(j) = a_j + 2b_j , \tag{3a}$$

$$A_{\perp}(j) = a_j - b_j , \tag{3b}$$

where

$$a_j = \tfrac{16}{3} \pi (\mu_j / I_j) \mu_B \alpha_j^2 \eta_j^2 |\phi_{3s}(0)|_j^2$$

and

$$b_j = \tfrac{4}{5} (\mu_j / I_j) \mu_B \beta_j^2 \eta_j^2 \langle r_{3p}^{-3} \rangle_j .$$

α_j^2 refers to the probability of the s wave at the jth nucleus and β_j^2 to that of the p wave; μ_B represents the Bohr magneton.

Using $(\mu_j / I_j) = -1.1106 \mu_N$ for Si^{29} and $|\phi_{3s}(0)|^2 = 31.5 \times 10^{24}$ cm^{-3}, $\langle r_{3p}^{-3} \rangle = 16.1 \times 10^{24}$ cm^{-3} estimated for the silicon atom from the Hartree-Fock wave function [Appendix A in Ref. (19)], we have calculated α_j^2, β_j^2, and η_j^2 at various temperatures from the experimental data listed in Table I, and the results are given in Table II. Also, Fig. 12 shows temperature dependence of both η_A^2 and η_B^2 from 77 to 325 °K. Here we also plot $\eta_A^2 + \eta_B^2$, the total wave function localized at both sites, which accounts for 61% of the wave function of the resonant electron, independent of temperature. However, η_A^2 varies with temperature from 40% at 325 °K to 61% at 77 °K, while η_B^2 decreases from 21% at 325 °K to 16% at 180 °K. This means that the hyperfine indicates directly that, as temperature increases, the electronic wave function which was originally localized in the dangling bond A at a low temperature flows from the nucleus A to the B within a defect. On the other hand, we can see from Table II that both α_j^2 and β_j^2 have not changed with temperature for both atoms A and B; i.e., $\alpha_j^2 \sim 10\%$ and $\beta_j^2 \sim 90\%$, regardless of the nuclear site (A or B). The enhanced p-like character over the tetrahedral sp^3 orbital (25% s wave, 75% p wave), which is

TABLE II. Hyperfine parameters (in units of 10^{-4} cm^{-1}) and wave-function coefficients of the P-1 center.

Temp. (°K)	a_A	b_A	α^2_A	β^2_A	η^2_A	a_B	b_B	α^2_B	β^2_B	η^2_B
320	55.6	12.8	0.10	0.90	0.40	28.6	6.47	0.10	0.90	0.21
300	56.7	13.2	0.10	0.90	0.41	27.2	5.80	0.10	0.90	0.20
273	58.3	13.6	0.095	0.905	0.42	25.3	5.6	0.10	0.90	0.18
250	59.5	13.9	0.10	0.90	0.43	24.2	5.2	0.10	0.90	0.175
230	61.6	14.4	0.10	0.90	0.45	22.7	3.80	0.12	0.88	0.16
210	62.7	14.6	0.10	0.90	0.454	21.6	3.80	0.12	0.88	0.156
200	63.8	15.2	0.093	0.907	0.462	20.3	3.8	0.11	0.89	0.15
180	65.6	15.0	0.10	0.90	0.48	17.6	4.4	0.09	0.91	0.14
160	71.3	15.4	0.10	0.90	0.52	• • •	• • •	• • •	• • •	• • •
120	82.1	18.0	0.10	0.90	0.59	• • •	• • •	• • •	• • •	• • •
110	81.6	19.1	0.095	0.905	0.62	• • •	• • •	• • •	• • •	• • •
77	81.2	18.9	0.095	0.905	0.62	• • •	• • •	• • •	• • •	• • •

common to the most defects associated with the dangling bonds around vacancies, could be interpreted in terms of a relaxation of the atoms A and B (see Fig. 7) away from the vacancy V_1 or V_3, and toward its three nearest neighbors, respectively; as a result each group of four atoms around the A and B atoms would have a tendency to form a planar configuration with sp^2 orbitals, leaving the pure p orbital directed along the ⟨111⟩ axis.

The C hyperfine satellite of the central line s at ⟨100⟩, the satellite of t_1 at ⟨111⟩ and that of u_1 at ⟨110⟩ are unambiguously measured to be 2.7, 2.6, and 2.3 G, respectively, at room temperature, and 4.5, 3.8, and 3.4 G, respectively, at 100 °K, which suggests that the A tensor of the set C is also anisotropic and temperature dependent. Since the hyperfine splitting varies little with orientation (it could be less than 1 G), we choose the largest separation at ⟨100⟩ as $A_{\parallel}$ and the smallest one at ⟨110⟩ as $A_{\perp}$. With this assumption, we have obtained $\alpha_c^2 \sim 32\%$, $\beta_c^2 \sim 68\%$, and $\eta_c^2 \sim 1.4\%$ for each nuclei, suggesting that the normal sp^3 hybrid orbitals participate in the interaction, and that ~10% of the wave function is accounted for on the six or seven atoms in the vicinity of the defect. We presume that the hyperfine structure C arises from those six atoms C, C', C'', D, D', and D'' in the defect model (see Fig. 7). We do not attempt here to take account of temperature variation of the set C, because our estimate already contains a significant error, dominating the small variation with temperature.

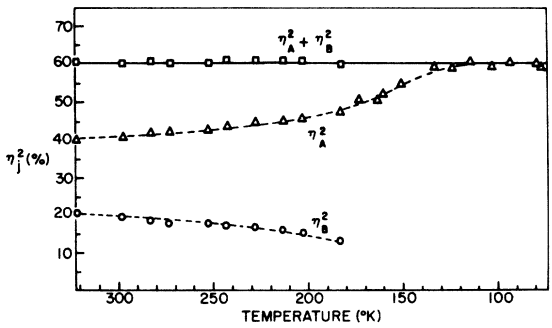

FIG. 12. Temperature dependence of the resonant wave function; η_A^2 is a fraction of the wave function at the A atom (triangles) and η_B^2 is that for the B atom (circles). The total fraction ($\eta_A^2 + \eta_B^2$) is always 0.61, independent of temperature.

Considering the three sets A, B, and C of the Si^{29} hyperfine structure, a total 70% of the wave function is localized in the atoms surrounding the five vacancies, and the remaining 30% we assume is spread over more remote atoms, giving contributions only to the breadth of a central line. Hence, our simple treatment in terms of localized molecular orbitals should be regarded as a reasonable first-order approximation.

Temperature dependence of the hyperfine interaction has previously been explained by the two distinct mechanisms: (a) a motional averaging process[19,20] and (b) a spin-lattice interaction.[21,22] In the latter case, the hyperfine structure is mainly affected by the lattice vibration of the host crystal in the vicinity of a paramagnetic center. The lattice vibration then changes the distance between the paramagnetic ion and its ligands, and as a result, the wave function of the paramagnetic electron varies with temperature, which leads to temperature dependence of the hyperfine structure and the other EPR parameters. This effect has been, in fact, observed in the F centers in alkali halides[22,23] by ENDOR measurements, and for Mn^{2+} and V^{2+} in MgO[24] and for Mn^{2+} in $CaCO_3$.[25] In these systems, the hyperfine constant decreases with increasing temperature, but the variation is less than a few percent over the temperature interval 4.2–800 °K, i.e., small compared to the P-1 variation.

Although the motional effect due to electron hop-

ping has been observed for simple radiation-induced defects in silicon, we have already ruled out the possibility of electron jumping between equivalent sites in the P-1 center by the absence of an average state between equivalent sites. Another source of temperature effect results from phonon-induced transitions connecting the ground state and nearby excited states of a paramagnetic center. The resonant electrons populate the ground and excited states according to the Boltzmann distribution, and when the transition is fast enough an averaged hyperfine interaction is observed, as in the case of the hyperfine interaction of the Li-donor state[26] and the P-donor state[20] in silicon where the hyperfine constant shows a strong dependence upon temperature.

Let us now consider what our model predicts will be the temperature dependence of the hyperfine spectra of the P-1 center due to transitions from the ground state to the first excited state. First, we note that we are concerned with the hyperfine structure due to one Si^{29} nucleus; those defects which have no Si^{29} will yield EPR spectra that will occur in the central lines, while those defects which have two Si^{29} nuclei will contribute a much less intense hyperfine spectra (as yet unobserved) which will appear at a much larger splitting from the central lines. There will be three distinct hyperfine spectra due to defects with one Si^{29} nucleus: (i) that due to the Si^{29} being in atom A of Fig. 8, (ii) in atom B, and (iii) in one of the atoms of the sets of atoms labeled C and D (this latter hyperfine spectra corresponds to the C spectrum and will not be considered further here). Consider first a defect which has a Si^{29} nucleus on atom A and consequently a Si^{28} (spin 0) nucleus on atom B. In the ground state the resonant electron is localized on atom A and the low temperature hyperfine line (the A line) will be observed. Transitions from the ground state to the first excited state will introduce a broadening on the A line leading to its disappearance with increasing temperature. When the transition rate gets fast enough the resonant electron becomes an average between the ground-state wave function (which corresponds to the A line) and the excited-state wave function. The resonance of the pure excited state is that of a Si^{28} nucleus, but shifted (slightly) from the central line due to the presence of the neighboring Si^{29} at the A site. The admixture of the excited state to the ground state is temperature dependent, the proportions being determined by the Boltzmann factor. Consequently with increasing temperature a new hyperfine line will appear, broad at first and then narrowing with increasing temperature, which corresponds to the hyperfine spectra for the averaged wave function. The intensity of this line *vis a vis* the central line will still correspond to a one silicon center, because the defect still involves just one Si^{29}, and all of the resonant intensity shows up in this hyperfine line (including of course the companion line on the other side of the central lines). Consider next the defect which has its Si^{29} on the B atom, and consequently a Si^{28} nucleus on the A atom. In the ground state the resonant electron is localized on the A atom and the resonance line again occurs near the central line (and is not resolved by us). With increasing temperature this line will similarly broaden and disappear and a new line will appear which reflects the averaged wave function between the ground state and the first excited state. In this case the first excited state involves a Si^{29} hyperfine interaction and an increasing admixture of that wave function with temperature will lead to a hyperfine line (the B line) which increasingly splits from the central line and hence is resolved. Again the intensity of this line *vis a vis* the central line will correspond to that of a one silicon center, because the defect has only one Si^{29} and all of the intensity appears in this hyperfine line.

The shift in position in the hyperfine lines with temperature reflects the temperature-dependent occupancy of the excited state. Since the Boltzmann factor for the defect with the Si^{29} at A is the same as that with it at B we can compare the ground state of the A defect to the excited state of the B defect. The ratio of the fraction η_j^2 of the resonant wave function in each energy state (i.e., the probability of finding the resonant electron at each state), will be given by

$$\eta_A^2/\eta_B^2 = e^{+\Delta/kT}, \tag{4a}$$

where $\Delta = E_1 - E_0$, i.e., the energy splitting between the ground state (E_0) and the excited state (E_1). In Fig. 13 we plot $\ln(\eta_A^2/\eta_B^2)$ against $1/T$ where we used our experimental estimates for η_j^2 deduced from the analysis of the hyperfine structure of the sets A and B and given in Table II. The experimental points lie along a straight line, indicating that the energy splitting Δ is 0.024 eV. We can also see this directly from the hyperfine splitting, since the hyperfine splittings in an arbitrary orientation should follow the same relationship, because the splitting is proportional to the amount of the electronic wave function at each state. That is

$$A_A(\theta)/A_B(\theta) = e^{+\Delta/kT}, \tag{4b}$$

where $A(\theta)$ represents the hyperfine separation from the corresponding central line, as the magnetic field axis is at θ° from the $\langle 110\rangle$ crystal axis. This dependence was examined at $\theta = 90^\circ$ (i.e., $\vec{H} \parallel \langle 100\rangle$) where we can observe the two hyperfine satellites. The results are also shown in Fig. 13, providing the same activation energy consistent with the one obtained from the indirect measurements of η_j^2.

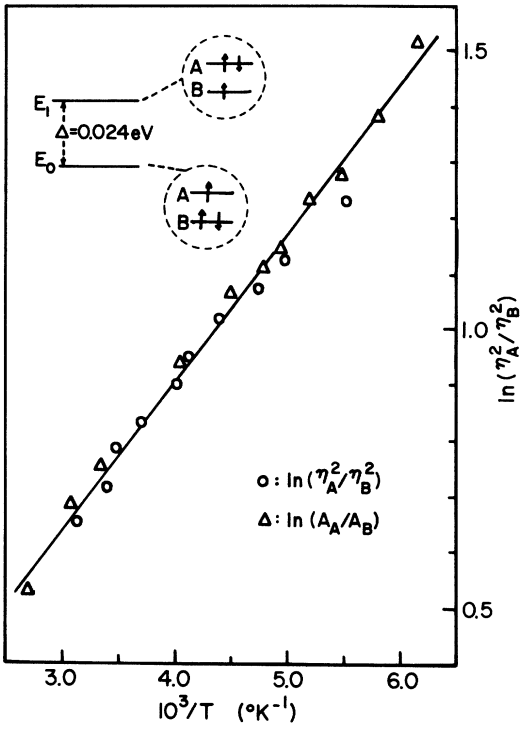

FIG. 13. Relative electronic population between the ground and excited states; the population was measured in two different ways, i.e., (a) from the estimates of η_A^2 and η_B^2 (circles) and (b) from direct measurements of the hfs splitting in <100> (triangles). The population ratio between these two states (E_0 and E_1) follows the Boltzmann statistics. Also, the electronic configurations are shown in the insets.

The hfs splitting A at the averaged state can be written as[26]

$$A = A_g p_g + A_e p_e , \tag{5}$$

where (A_g, A_e) refers to the hyperfine separation at the ground and excited states and (p_g, p_e) are the probability of the corresponding states. Since $\eta_A^2 + \eta_B^2 = 0.61$, both p_g and p_e can be obtained by normalizing the experimental values of η_A^2 and η_B^2; i.e., $p_g = \eta_A^2/0.61$ and $p_e = \eta_B^2/0.61$. Thus, one can estimate A_e in the excited state from the known A_g at 77 °K. We made calculations for both defects A and B at $\vec{H} \parallel \langle 100 \rangle$ by using the hfs splittings given in Fig. 5 and η_A^2, η_B^2 in Table II; A_e of the defect A is $\sim 0.2 \pm 0.2$ G, independent of temperature and A_e of the defect B is approximately 46 G, comparable to A_g (= 47 G) in the A site. This is consistent with the model we used to describe the motional effect.

Consider now the line broadening in the hyperfine satellites. As we can see from the actual EPR signal lines in Fig. 11, the peak-to-peak breadth starts to increase near 200 °K, as temperature lowers and, at 150 °K, reaches a maximum (ΔH_{pp} ~ 5 G) of a factor of 2 larger than the width at room temperature. In the temperature range below 150 °K down to 77 °K, the hyperfine linewidth narrows gradually, finally, at 77 °K, being equal to the one at 300 °K. One can estimate the lifetime (τ_e) of the excited state from the equation[26]

$$\tau_e = 4/T_2(\delta\omega)^2[1 - (p_g - p_e)^2]\, p_g \tag{6}$$

for the averaged line, where $\delta\omega = g\mu_B(A_g - A_e)/\hbar$ and T_2 can be obtained from the linewidth. Since the peak-to-peak width was actually measured, it was first converted to the half-width by assuming two different line shapes: $\Delta H_{1/2} = (2\ln 2)^{1/2}\Delta H_{pp}$ for the Gaussian shape and $\Delta H_{1/2} = (3)^{1/2}\Delta H_{pp}$ for the Lorentzian; and then T_2 was obtained with the two methods: $T_2 = [\Delta\omega^2 - (\Delta\omega_0)^2]^{-1/2}$ for the Gaussian and $T_2 = [\Delta\omega - (\Delta\omega_0)]^{-1}$ for the Lorentzian line shape. Since the correct behavior may be somewhere in between these two simple approaches, we have simply averaged the two estimates. With the estimates, $T_2 \sim 5\times10^{-8}$ sec and $\delta\omega \sim 8\times10^{8}$/sec near 200 °K where the reliable values of p_g and p_e are available, the lifetime in the excited state is in the order of 10^{-10} sec, consistent with the requirement of the motional averaging ($\tau_e\delta\omega \ll 1$).

The intensity of the hyperfine satellites is so small (about 2.4% of that of the central line) that a high modulation was required to measure the width without ambiguity. Thus, we could not avoid an additional broadening due to the high modulation. Also, the accuracy was limited by superposition of a pair of satellites, when the linewidth broadens severely. Therefore, we could not use the linewidth to obtain the activation energy of the transition to the excited state with reliability.

We conclude that the temperature dependence of the EPR parameters is explained satisfactorily by the phonon-induced motional effect between the ground and first excited electronic states. In view of our defect model, the temperature effect is a natural consequence of the electronic structure of the defect, so that this must be regarded as important support of the model.

D. g Tensor

1. Low Temperature

We have shown that, at 77 °K, 61% of the wave function is located in a broken bond of the A atom in Fig. 7, and that the g tensor is approximately axially symmetric about the $\langle 111 \rangle$ axis, the bond axis described by $\vec{A}_{\parallel}$. Since the situation seems very similar to the case of the G-8 spectrum, we will follow the simple treatment, developed by Watkins and Corbett,[19] for a quantitative analysis of the g tensor arising from an unpaired dangling bond of a silicon atom.

The general expression for the g shift is given by the perturbation theory as

$$\Delta g_{ij} = 2\sum_n \frac{\langle 0|(\vec{V}_{SO})_i|n\rangle\langle n|L_j|0\rangle}{E_0 - E_n}, \quad (7)$$

where $\vec{V}_{SO} = (\mu_B/mc)\vec{E}\times\vec{p}$ is the spin-orbit coupling. $\vec{E}$ represents the electric field through which an electron is moving, $\vec{p}$ the linear momentum and $\vec{L}$ the angular momentum of electron. Due to axial symmetry of the molecular-orbital (MO) orbital of a dangling bond, as argued in Ref. 19, the matrix element $\langle n|L_j|0\rangle$ has no contribution along the bond axis. Thus, $\Delta g_{\parallel}$ will be zero, but $\Delta g_{\perp}$ may be expected a finite shift. Taking account of the coupling between the atom associated with a dangling bond and its three nearest neighbors, they derived the equation for the g shift in $g_{\perp}$ (for detailed derivations, see Appendix B in Ref. 19);

$$\Delta g_{\perp} = \lambda_{3p}\left(\frac{1+\gamma}{E_b} - \frac{1-\gamma}{E_a}\right)\beta_A^2, \quad (8)$$

where γ is a scale factor for the overlap between the valence and core wave functions, which was estimated to be $+0.17$ for the normal Si-Si lattice distance and with the tetrahedral sp^3 hybrids. λ_{3p} is the spin-orbit coupling constant for the $3p$ atomic wave function and β_A^2 a fraction of $3p$ character obtained experimentally from the hyperfine structure.

The observed g shift of the G-8 spectrum was $\Delta g_{\parallel} = -0.0018$ and $\Delta g_{\perp} = +0.0081$. After making corrections for the g shift in $g_{\parallel}$ and for the fact that 40% of the wave function is missing, they deduced $\Delta g_{\parallel} = 0$ and $\Delta g_{\perp} = 0.017$ for a dangling bond in which the full electronic wave function is localized. With their estimate of parameters, $E_b = 1.5$ eV, $E_a = 2.5$ eV, $\lambda_{3p} = 0.02$ eV, and $\beta_A^2 = 0.86$, Eq. (8) gives only $\Delta g_{\perp} = 0.008$, a factor of 2 smaller than that to be expected by experiment. They reasoned that this discrepancy may arise from neglecting "compression" of the valence-band wave function which could enhance the spin-orbit interaction, and that the scale factor γ of the core wave function was changed from 0.17 to 0.8 to meet the experimental value. Phillips[27] introduced this effect into Eq. (8) in such a way that compression of $3p$-bonding states gives rise to an increase in the spin-orbit coupling constant of bonding orbitals over the conduction-band antibonding orbitals. Thus, he argued that Eq. (8) should be changed to

$$\Delta g_{\perp} = \left(\lambda_b\frac{1+\gamma}{E_b} - \lambda_a\frac{1-\gamma}{E_a}\right)\beta_A^2, \quad (9)$$

where λ_b represents the spin-orbit coupling constant for the bonding orbitals and λ_a for the antibonding orbitals. With $\lambda_b = 0.029$ eV from piezospectroscopic data and $\lambda_a \simeq \frac{1}{2}\lambda_b = 0.015$ eV, he obtained $\Delta g_{\perp} = 0.02$, which explains satisfactorily the experimental estimate of the G-8 spectrum.

Let us now consider the g tensor of the P-1 center at 77 °K. The measured g shifts are $\Delta g_{\parallel} = -0.0003$ and $\Delta g_{\perp} = +0.0088$, which is rather close to the general requirement (i.e., $\Delta g_{\parallel} = 0$) compared with G-8. From the presumption that the small negative g shift in $g_{\parallel}$ arises from 39% of the wave function not localized in a broken bond, we obtain $\Delta g_{\parallel} = 0$ and $\Delta g_{\perp} = 0.0091$ for the bond that occupies only 61% of the total wave function. Then, the fully occupied dangling bond should provide the g shift $\Delta g_{\parallel} = 0$ and $\Delta g_{\perp} = 0.015$. It is very difficult to estimate E_a and E_b of the P-1 center, but we know that the localized level of the defect should be somewhere in between $(E_c - 0.4)$ eV of G-8 and the middle of the forbidden band. This can be seen from the fact that, in neutron-irradiated silicon, the G-8 spectrum appears only in the sample of low fluence ($\sim 10^{17}$ n/cm^2) but the P-1 center can be observed[6] in the case of higher fluence ($\sim 10^{18}$ n/cm^2). We therefore simply adopt the estimates for G-8 and Eq. (9) gives $\Delta g_{\perp} = +0.015$, which is in excellent agreement with the experimental estimate. This is reasonable considering the fact that the P-1 center, an intrinsic defect with a single dangling bond left alone in a large space of vacancy cluster, would fit much better to the simple model (see Fig. 8 of Ref. 19) for the g-shift calculation than does G-8. As Elkin and Watkins pointed out,[11] the spin-orbit interaction at a nearby impurity atom (as in G-8) gives rise to a further distortion in the g tensor from axial symmetry, because the spin-orbit coupling of an impurity may be strong enough to perturb the electric field seen by the resonant electron. Since $\lambda(\mathrm{P}) \simeq \lambda(\mathrm{Si})$, however, the phosphorus atom may influence less to the g-tensor distortion and as a result, for the G-8 center, satisfactory agreement can be achieved from this simple model. Therefore, this analysis of P-1 supports the view that a single broken bond orbital in silicon gives rise to the g shifts $\Delta g_{\parallel} = 0$ and $\Delta g_{\perp} \simeq 0.017$, when the wave function of a resonant electron is completely localized in the dangling bond.

2. High Temperature

We have shown from the hyperfine structure that, as the temperature increases, the wave function spills over from the A atom to the B atom, and as a result, two dangling bonds participate in spin resonance.

Let us now consider a simple treatment of the g shift arising from the two dangling bonds (A and B) whose energy levels differ slightly from each other and determine what we expect if the resonant electron makes fast transition between these two levels, as the temperature increases. Since the main contribution to the g shift stems from the spin-orbit interaction, we have to calculate the g shifts at the two different energy states separately and then to take the average between them to obtain the g shift in the averaged state. In other words, as soon as

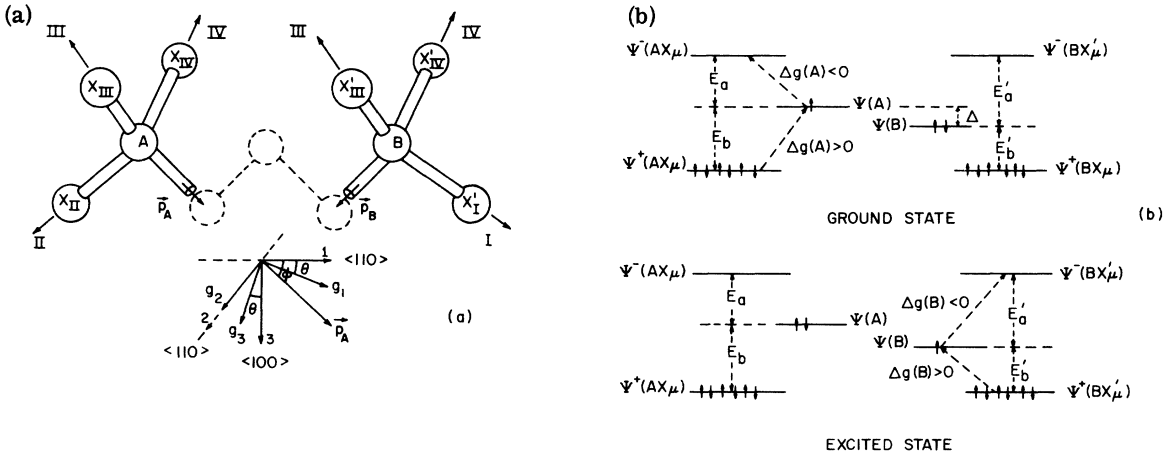

FIG. 14. The model used to calculate the g shifts at the high temperature; (A) the simplified atomic configuration in the defect and the geometry of the coordinate system. I, II, III, and IV indicates the directions toward three surrounding atoms from the atoms A and B. The resonant wave function is localized in the two dangling bonds of A and B. $\vec{p}_A$ and $\vec{p}_B$ represent the direction of p wave in the dangling bond orbitals A and B, respectively. (B) Schematic energy diagram. The electronic transitions are shown for the ground and excited states. The energy level of $\Psi(B)$ is lower than the one for $\Psi(A)$ to satisfy the defect model of the P-1 center.

the resonant electron jumps up to the excited B state (the dangling bond at the B atom), it experiences the corresponding spin-orbit interaction, prior to coming back to the ground A state (the dangling bond at the A atom). As a result, the g tensor depends strongly on the energy state where the resonant electron resides at a particular time. Therefore, what we observe in the motionally averaged state is the appropriately averaged value of the two distinct g tensors belonging to the dangling bond of atoms A and B, respectively.

Figure 14 shows a simple model which consists of the two atoms (A and B) and of their six nearest neighbors. The atom A couples strongly with its three neighbors, X_{II}, X_{III}, and X_{IV}, and similarly for the B atom. In light of our defect model, three vacancies are between the atoms A and B so that the two dangling bonds make the angle ~109°. We assume a three-vacancy string would be large enough to ignore a coupling between the atom A and the nearest neighbors of the atom B, and correspondingly for atom B. To first order therefore, we can treat the problem as one dangling bond which interacts only with three surrounding neighbors, as shown in Fig. 14(b).

Since our treatment is very similar to the one used by Watkins[19] in deriving Eq. (8), we will adopt his notations. We set up the approximate LCAO-molecular orbitals for the ground state in terms of four orthogonal atomic orbitals σ_3^μ (μ = I, II, III, IV) and the core functions ϕ_i^μ:

$$\Psi(A)=\sigma_3^{\mathrm{I}}(A)=\alpha_A^{\mathrm{I}}\phi_{3s}(A)+\beta_A^{\mathrm{I}}\phi_{3p}(A), \tag{10a}$$

$$\Psi^{\pm}(AX_\mu)=N^{\pm}\left(\sigma_3^\mu(A)\pm\sigma_3^{-\mu}(X_\mu)\mp\sum_i\epsilon_i[\phi_i(A)\pm\phi_i(X_\mu)]\right),\quad \mu=\mathrm{II},\ \mathrm{III},\ \mathrm{IV}, \tag{10b}$$

where the superscript μ indicates the direction of orbitals as shown in Fig. 14 and the subscript μ refers to the position of three nearest neighbors. The core function ϕ_i's are constructed from 1s, 2s, and 2p atomic wave functions, and the normalization constants are

$$N^{\pm}=\left[2\left(1\pm S-\sum_i\epsilon_i^2\right)\right]^{-1/2}$$

with

$$S=\langle\sigma_3^\mu(A)\,|\,\sigma_3^{-\mu}(X_\mu)\rangle,$$

$$\epsilon_i=\langle\sigma_3^\mu(A)\,|\,\phi_i(X_\mu)\rangle=\langle\sigma_3^{-\mu}(X_\mu)\,|\,\phi_i(A)\rangle.$$

Similarly, we have for the excited state (the dangling bond at the B atom)

$$\Psi(B)=\sigma_3^{\mathrm{II}}(B)=\alpha_B^{\mathrm{II}}\phi_{3s}(B)+\beta_B^{\mathrm{II}}\phi_{3p}(B), \tag{11a}$$

$$\Psi^{\pm}(BX'_\mu)=N^{\pm}\left(\sigma_3^\mu(B)\pm\sigma_3^{-\mu}(X'_\mu)\mp\sum_i\epsilon_i[\phi_i(B)\pm\phi_i(X'_\mu)]\right),\quad \mu=\mathrm{I},\ \mathrm{III},\ \mathrm{IV}. \tag{11b}$$

By substituting the LCAO-MO orbitals in Eqs. (10) and (11) into Eq. (7) with the similar manipulations to those done in Ref. 19, we have obtained the g shift in the unprimed coordinates shown in Fig. 14: for the ground state,

$$\Delta g_{ij}(A)=\left(\lambda_b\frac{1+\gamma}{E_b}-\lambda_a\frac{1-\gamma}{E_a}\right)\langle\sigma_3^{\mathrm{I}}(A)\,|\,L_iL_j\,|\,\sigma_3^{\mathrm{I}}(A)\rangle. \tag{12}$$

Similarly, we have for the excited state

$$\Delta g_{ij}(B)=\left(\lambda_b\frac{1+\gamma}{E_b'}-\lambda_a\frac{1-\gamma}{E_a'}\right)\langle\sigma_3^{II}(B)\,|\,L_iL_j\,|\,\sigma_3^{II}(B)\rangle\,. \tag{13}$$

Here, we approximate $\gamma_a\simeq\gamma_b\simeq\gamma$, because such terms only contribute small corrections, negligible compared with other unknown parameters like E_a and E_b. Using the conventional expression of the angular momentum operator and the bond directions, $\vec{P}_A$ and $\vec{P}_B$, with respect to the unprimed coordinate system, the matrix element in Eqs. (12) and (13) can be easily calculated, and the final results (in matrix form) are obtained:

$$\overleftrightarrow{\Delta g}(A)=K\begin{pmatrix}\sin^2\phi & 0 & -\sin\phi\cos\phi\\ 0 & 1 & 0\\ -\sin\phi\cos\phi & 0 & \cos^2\phi\end{pmatrix}$$

$$=\frac{K}{3}\begin{pmatrix}1 & 0 & -\sqrt{2}\\ & 3 & 0\\ & & 2\end{pmatrix} \tag{14a}$$

and

$$\overleftrightarrow{\Delta g}(B)=\frac{K'}{3}\begin{pmatrix}1 & 0 & \sqrt{2}\\ & 3 & 0\\ & & 2\end{pmatrix}\,, \tag{14b}$$

where we made use of the fact that the hyperfine axes at both A and B sites are always along the $\langle111\rangle$ axis (i.e., $\cos^2\phi=\frac{2}{3}$), and

$$K=\left(\lambda_b\frac{1+\gamma}{E_b}-\lambda_a\frac{1-\gamma}{E_a}\right)\beta_A^2,$$

$$K'=\left(\lambda_b\frac{1+\gamma}{E_b'}-\lambda_a\frac{1-\gamma}{E_a'}\right)\beta_B^2\,.$$

From experiment, $\beta_A^2=\beta_B^2=0.90$ but $E_b\neq E_b'$ and $E_a\neq E_a'$, so that K is, in general, not equal to K'.

Let p_g and p_e be the probability in the ground and excited states, respectively, as defined in Eq. (5) (Sec. IV C). The g shift in the motionally averaged state can be written as

$$\langle\overleftrightarrow{\Delta g}\rangle=p_g\overleftrightarrow{\Delta g}(A)+p_e\overleftrightarrow{\Delta g}(B)$$

$$=\frac{1}{3}\begin{pmatrix}p_gK+p_eK' & 0 & -\sqrt{2}(p_gK-p_eK')\\ & 3(p_gK+p_eK') & 0\\ & & 2(p_gK+p_eK')\end{pmatrix} \tag{15}$$

Since we already know from Eq. (15) the g_2 axis in the direction perpendicular to the symmetry plane of the defect (the 2 axis), we can easily diagonalize the matrix $\langle\overleftrightarrow{\Delta g}\rangle$ to obtain the g_1 and g_3 principal axes by rotating the unprimed system by the distortion angle ($\theta°$) with respect to the g_2 axis. From the transformation of ($\overleftrightarrow{\Delta g}$) into the principal axes system in which the diagonal elements represent the g shift in the principal axes, and the off-diagonal terms are zero, the distortion angle can be derived as

$$\theta=\tfrac{1}{2}\tan^{-1}\left(\sqrt{8}\,\frac{p_gK-p_eK'}{p_gK+p_eK'}\right)\,. \tag{16a}$$

The results of the g shifts in the principal axis system are

$$\Delta g_1=\tfrac{1}{3}[(p_gK+p_eK')(2-\cos^2\theta)$$
$$-\sqrt{8}\,(p_gK-p_eK')\cos\theta\sin\theta]\,, \tag{16b}$$

$$\Delta g_2=p_gK+p_eK' \tag{16c}$$

$$\Delta g_3=\tfrac{1}{3}[(p_gK+p_eK')(1+\cos^2\theta)$$
$$+\sqrt{8}\,(p_gK-p_eK')\cos\theta\sin\theta]\,. \tag{16d}$$

We note that the g shifts (Δg_i) and the distortion angle (θ) must vary continuously with temperature, because of the temperature dependence of both p_g and p_e (i.e., $p_g/p_e=e^{\Delta/kT}$). At 77 °K where $p_g=1$ and $p_e=0$, Eqs. (16) provide $\theta=35.3°$ (i.e., $\vec{g}_1\parallel\langle111\rangle$), $\Delta g_1=0$ and $\Delta g_2=\Delta g_3=K$, which is Eq. (9) used in Sec. IV D 1 to analyze the g tensor at the low temperature. As $T\to\infty$, $p_g\simeq p_e$; i.e., the two dangling bonds become symmetric as in the case of the B-1 center; under that circumstance, Eqs. (16) give $\theta=0°$ and $\Delta g_2:\Delta g_3:\Delta g_1=3:2:1$, consistent with the previous result[10] of the g-tensor analysis for the C_{2v}-symmetric pair bond. Therefore, our results provide the qualitative features of the g tensor in the case of one dangling bond as well as of the symmetric pair bond.

Using Eqs. (16), we will calculate the g tensor as a function of temperature. Since we are dealing with the g shift arising from only 61% of the total resonant wave function, Δg_i in Eqs. (16) that is due to the 100% wave function should be multiplied by 0.61 to obtain the actual values of the g tensor. For simplicity of calculation, we also approximate η_A^2 ($=0.61\times p_g$) in Table II giving $\eta_A^2\simeq 0.32e^{73.96/T}$, which fits the experimental data reasonably well. We notice that the temperature dependence of Δg_2 is very sensitive to the choice of the most uncertain parameters: E_a, E_b, E_a', and E_b'. We determined $K=0.0153$ and $K'=0.0188$ from the measurements of Δg_2 [Fig. 4(b)] at 100 and 300 °K where reliable p_e and p_g are available from the hyperfine structure. Both K and K' so obtained can be regarded reasonable, because the g-tensor analysis of the dangling bond at 77 °K (Sec. IV D 1) showed that K (identical to $\Delta g_\perp$ at low temperature) ranges from 0.015 to 0.020. With the parameters, K, K', and η_A^2, given above and $p_g+p_e=1$, we calculate the distortion angle and g principal values from Eqs. (16); the results are presented in Fig. 4. Good agreement is achieved in the distortion angle, and

the qualitative trend of g_1 and g_3 obtained. Further refinement in the model can accommodate the remaining discrepancies, but at the cost of introducing additional empirical parameters. For example, the model assumes a threefold, axially symmetric $\langle 111 \rangle$ dangling bond, but in detail g_2 is only approximately equal to g_3 at low temperatures. The fact that $g_2 \neq g_3$ implies a lack of equivalence of the neighboring atoms, i.e., additional corresponding K and K' parameters. [This same lack of equivalence is evident in other C_{1h} defects: the divacancy[18] (G-6 and G-7), the vacancy-phosphorus pair[19] (G-8), and the four-vacancy[4] (P-3).] But there are additional factors also not contained in the simple model presented here; for example, the contribution of the wave function not localized on the immediate neighbors, thermal vibrations, etc. A much more extensive and rigorous theoretical calculation is required to fully treat the present center and the rest of the silicon centers. We feel the present treatment incorporates the essential physics and is in sufficient detail to validate the identification of the center as due to a five-vacancy defect.

We also note that, if the P-1 center were in a positive charge state (a lack of one electron), the energy level of $\Psi(A)$ would be lower than that of $\Psi(B)$ and K should be larger than K' because $\Psi^{\pm}(AX_{\mu})$ is equivalent to $\Psi^{\pm}(BX'_{\mu})$; but our estimates indicate $K' > K$. Therefore, again we conclude that the P-1 spectrum arises from a negative charge state as predicted in Fig. 9.

E. Stress Alignment

The response of EPR spectra to an externally applied uniaxial stress provides additional information concerning the defect structure. The applied stress disturbs the normal cubic symmetry of the crystal and as a result, the six equivalent sites of the $\langle 110 \rangle$ symmetric defects such as the P-1 center are no longer in equal energy states; if reorientation can take place, those defects with different orientations no longer yield central lines of equal intensity.

It has been found[10] in the radiation-induced defect centers in silicon that the change in relative intensities among the central lines due to a uniaxial stress can arise from two different mechanisms; either electronic bond-switching motion or reorientation of defects themselves, depending on the temperature region in which experiment is performed.

The EPR measurements in the stress study were performed at 300 °K on a sample annealed at 400 °C where the spectrum is primarily P-1 and is most free of lines due to other centers. For a compressive stress applied along the $\langle 110 \rangle$ direction at 300 °K, the P-1 spectrum was not altered either in g value, hyperfine or angles, even at our maximum pressure (3000 kg/cm^2). Although our defect model (Fig. 7) does not permit any transition from one defect site to another by a simple electronic bond-switching motion, we expect that, since the wave function is so sensitive to temperature that a small change in $E_A - E_B$ could result in a detectable variation in the hyperfine structure as well as the g tensor. Apparently these levels respond together to a given stress.

A preferential alignment of the defects was achieved by applying a compressional stress at an elevated temperature. In this experiment, an unannealed sample in which the P-1 spectrum was initially absent, was heated for 2 h under 2200-kg/cm^2 compression along the $\langle 110 \rangle$ direction, until temperature increased to 225 °C. During this period, the P-1 center was created along with other spectra, A-2, A-3, A-4 and A-6. When the temperature reached at 225 °C, it was kept constant for 30 min and then the sample temperature was lowered to room temperature in 30 min with stress on. After releasing the pressure, the sample was removed from the oven and placed in the 35-GHz cavity for room-temperature measurements. We have observed a considerable alignment among the differently oriented defect sites monitored by the relative intensity of the corresponding central lines.

The results are shown in Fig. 15; the measurements were made with the magnetic field parallel to the $\langle 110 \rangle$ axis; (a) with zero stress and (b) after applied the pressure at the high temperature. Here, each central line is labeled in terms of the notation used by Watkins *et al.*[10,19] to designate the orientation of the corresponding defect with respect to the $\langle 110 \rangle$ stress axis. The defects *ad* (*a* and *d* represent the positions of the atoms *A* and *B* at the corner of the cubic lattice) and *bc* have their $\{110\}$ symmetry plane perpendicular to and parallel to the uniaxial stress, respectively, and those of *ab*, *ac*, *bd*, and *cd* refer to the one whose $\{110\}$ sym-

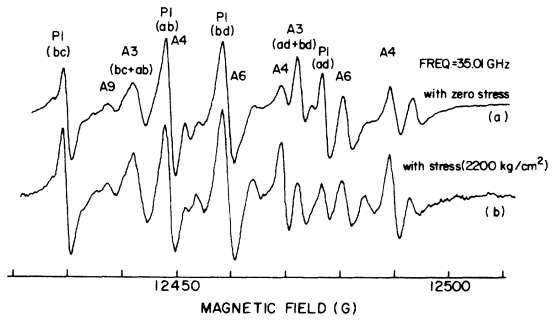

FIG. 15. Anisotropic alignment of differently oriented equivalent defects in the P-1 spectrum; the preferential alignment can be seen at the line *bc*, whose intensity increases after stress annealing.

metry plane forms 60° with the stress axis. Thus, the fine structure line u_1 with $\vec{H} \parallel \langle 100 \rangle$ (see Fig. 2) indicates the concentration of the defect bc (N_{bc}), the line u_2 that of ab and ac ($N_{ab} = N_{ac}$), the line u_3 that of bd and cd ($N_{bd} = N_{cd}$) and the line u_4, ad (N_{ad}).

We observed that a quenched-in alignment takes place favoring the defect whose symmetry plane is parallel to the stress direction; i.e., $N_{bc} > N_{ab} > N_{ad}$. The degree of alignment defined as

$$\frac{n_{\parallel}}{n_{\perp}} = \frac{N_{bc} + N_{ba} + N_{bd}}{N_{ad} + N_{ac} + N_{ab}}$$

is estimated to be 1.37 for the P-1 center. The same experiment was also performed at both 455 and 555 °K with a different procedure; the sample was first annealed at a given temperature for 45 min to create the P-1 center under zero stress and then was compressed with 2000 kg/cm^2 for additional 30 min, retaining the same temperature. At both temperatures, the results are the same as before (i.e., $n_{\parallel}/n_{\perp} > 1$). This supports the view that the preferential alignment is achieved by the defect reorientation through atomic motion. We note that the alignment observed in the P-1 center is strikingly different from the previous observation[18,19] $n_{\parallel}/n_{\perp} < 1$ (i.e., $N_{ad} > N_{ab} > N_{bc}$) on the $\langle 110 \rangle$ "linear" defects such as the divacancy or four-vacancy centers. The opposite sense of alignment of the P-1 center from that of the "linear" defects argues that the P-1 is generically different from those defects which is consistent with the cluster-type defect of our model. Further details of the quantitative results will be published in the near future.

V. SUMMARY AND CONCLUSIONS

The P-1 is known to arise from one of the dominant defects in heavily damaged silicon; it can be only formed after heat treatment at 170 °C and is stable up to the 450 °C annealing. Both g and A tensors strongly depend upon temperature, and the temperature studies of the EPR parameters lead us to the following conclusions.

(a) The P-1 spectrum arises from a negatively charged state of a five-vacancy cluster. The defect structure is such that three vacancies are aligned in a row along the $\langle 110 \rangle$ axis and two more vacancies are arranged at both sides of the end one so that the $\{110\}$ symmetry is retained.

(b) The electronic structure is described primarily in terms of one-electron LCAO-molecular orbitals associated with the twelve lattice atoms surrounding the five vacancies. The resonant state is identified as consisting of admixtures of the states corresponding to the two broken bonds attached to the atoms A and B in Fig. 7.

(c) Analysis of the Si^{29} hyperfine structure indicated that, at 77 °K, roughly 61% of the electronic wave function is localized in a single dangling bond associated with the atom A and an additional 10% of the wave function contributes to the hyperfine interaction with the six (or seven) near neighbors. The rest of 30% is presumably spread over to the remote atoms in the vicinity of the defect center. As the temperature increases, the portion of the resonant wave function on the A atom flows to the B atom located at the other end of the three-vacancy string. At a high temperature, therefore, the wave function of a resonant electron is an average between the states corresponding to these two atoms, the relative portions given by the Boltzmann factor.

(d) The motional effect due to the electron hopping between differently oriented defect sites, as proposed in the previous study by Nisenoff and Fan, has not been observed in the present experiment. We find a temperature effect involving an electronic transition between the ground and excited states, which provides satisfactory explanation for the g-tensor variation with temperature. The energy separation between the ground and first excited states is deduced to be 0.024 eV.

(e) We do not observe a preferential alignment under external stress at 300 °K, but do observe an alignment on annealing under stress at 500 °K. A high-temperature alignment further supports the model of the defect as a cluster-type defect.

ACKNOWLEDGMENTS

We wish to express our appreciation to Dr. John Cleland (Oak Ridge National Laboratory) and Dr. Y. Y. Chu (Brookhaven National Laboratory) for their aid in the neutron irradiations, to Dr. Y. M. Kim for valuable suggestions and comments in the early stage of this work, to Dr. G. D. Watkins and Dr. F. S. Ham for very helpful conversations, and to the Dow Corning and Monsanto Companies for supplying the sample material.

---

†Research reported in this paper was supported in part by the Office of Navel Research under Contract No. N00014-70-C-0296

*Work in partial fulfillment of the requirements for the Ph.D. thesis by Y. H. Lee submitted to SUNY/Albany.

[1]G. D. Watkins, in *Proceedings of the Seventh International Conference on the Physics of Semiconductors: Radiation Damage in Semiconductors* (Dunod, Paris, 1964) p. 97.

[2]J. W. Corbett, in *Solid State Physics*, edited by F. Seitz and D. Turnbull (Academic, New York, 1966), Suppl. 7.

[3]M. Nisenoff and H. Y. Fan, Phys. Rev. **128**, 1605 (1962).

[4]W. Jung and G. S. Newell, Phys. Rev. **132**, 648 (1963).

[5]W. Jung, Ph.D. thesis (Purdue University 1963) (unpublished).

[6]Y. H. Lee, Y. M. Kim, and J. W. Corbett, Radiat. Eff. **15**, 77 (1972).

[7]Y. H. Lee, Ph.D. thesis (SUNY/Albany, 1972) (unpublished).

[8]D. F. Daly and K. A. Pickar, Appl. Phys. Lett. **15**, 267 (1969).
[9]D. F. Daly, J. Appl. Phys. **42**, 864 (1971).
[10]G. D. Watkins and J. W. Corbett, Phys. Rev. **121**, 1001 (1961).
[11]E. L. Elkin and G. D. Watkins, Phys. Rev. **174**, 881 (1968).
[12]H. Horiye and E. G. Wikner, J. Appl. Phys. **40**, 3879 (1969).
[13]B. Goldstein, Phys. Rev. Lett. **17**, 428 (1966).
[14]B. Goldstein, Radiat. Eff. **8**, 229 (1971).
[15]H. Lütgemeier and K. Schnitzke, Phys. Lett. A **25**, 232 (1967).
[16]K. L. Brower, Phys. Rev. B **4**, 1968 (1971).
[17]K. L. Brower, J. Appl. Phys. **43**, 3499 (1972).
[18]G. D. Watkins, and J. W. Corbett, Phys. Rev. **138**, A543 (1965).
[19]G. D. Watkins and J. W. Corbett, Phys. Rev. **134**, 1359 (1964).
[20]D. E. Dugdale, S. D. Lacey, and G. Lancaster, J. Phys. C **4**, 654 (1971).
[21]E. Simanek and R. Orbach, Phys. Rev. **145**, 191 (1966).
[22]V. Ya. Kravchenko and V. L. Vinetskii Opt. Spektrosk. **18**, 73 (1965) [Opt. Spectrosc. **18**, 37 (1965)].
[23]S. S. Ishchenko and N. P. Baran, Fiz. Tverd. Tela **11**, 1617 (1969) [Sov. Phys.-Solid State **11**, 1311 (1969)].
[24]W. M. Walsh, Jr., J. Jeener, and N. Bloembergen, Phys. Rev. 139, A1338 (1965).
[25]R. A. Serway, Phys. Rev. B **3**, 608 (1971).
[26]G. D. Watkins and F. S. Ham, Phys. Rev. B **1**, 4071 (1970).
[27]J. C. Phillips, Comments Solid State Phys. **3**, 67 (1970).